European Radiology (2019) 29:3441–3449
https://doi.org/10.1007/s00330-019-06226-4

MUSCULOSKELETAL

# Magnetic resonance imaging features of fibromas and giant cell tumors of the tendon sheath: differential diagnosis

Yuxi Ge[1] · Gang Guo[2] · Yaqian You[3] · Yunzhi Li[4] · Yinghua Xuan[3] · Zhe-Wu Jin[3] · Gen Yan[1,2]

Received: 18 February 2019 / Revised: 3 April 2019 / Accepted: 4 April 2019 / Published online: 30 April 2019


## Abstract

**Purpose** The clinical and imaging characteristics of fibromas of the tendon sheath (FTS) closely resemble those of giant cell tumors of the tendon sheath (GCTTS). We aimed to study MRI features of FTS and GCTTS to distinguish the two entities and improve their differential diagnosis.

**Materials and methods** We retrospectively analyzed data from 18 patients (9 men, 9 women; age, 17–62 years) and 24 patients (13 men, 11 women; age, 15–67 years) treated between May 2011 and May 2016, with histologically confirmed FTS and GCTTS, respectively. Specific MRI features of the two groups were compared using the independent sample *t* tests and chi-square tests.

**Results** FTS exhibited round or oval shapes. Proton-weighted images (PDWI) showed heterogeneous hypointensity that appeared striped or disordered and was located in the lesion center. Enhanced scans demonstrated asymmetrical signal in the foci. GCTTS mostly exhibited a lobulated or casting mold pattern, with a hypointense ring on PDWI. The hypointense components appeared granular/flaky or separated, sometimes behaving as a uniform signal on PDWI. Significant differences in the following features were observed between the two groups: lesion morphology ($p < 0.001$); imaging features on PDWI, including whether the signal is homogeneous ($p < 0.001$); the presence of a hypointense ring ($p = 0.006$); the location and morphology of hypointensity ($p < 0.001$); bone absorption ($p = 0.008$); enhancing pattern ($p = 0.008$); and whether the tumor crossed the joint ($p = 0.026$).

**Conclusions** FTS and GCTTS demonstrate distinctive MRI features, which can be used for differential diagnosis with sensitivities, specificities, and diagnostic accuracies of 83–100%, 29–79%, and 60–89%, respectively.

**Key Points**

- *Fibromas and giant cell tumors of the tendon sheath have distinct features on MRI, including differences in lesion morphology and intensity patterns, which can be used for differential diagnosis.*
- *Among other signs, GCTTS are more uniform than FTS, and FTS have a striped or disordered pattern.*
- *Tumors were classified with 90% accuracy into either FTS or GCTTS based on a combination of two features: homogenous signal and hypointensity shape on PDWI.*

**Keywords** Fibroma · Giant cell tumors · Magnetic resonance imaging

**Abbreviations**

| | |
|---|---|
| FTS | Fibromas of the tendon sheath |
| GCTTS | Giant cell tumors of the tendon sheath |
| PDWI | Proton density-weighted imaging |
| T1WI | T1-weighted spin-echo imaging |
| T2WI | T2-weighted spin-echo or fast spin-echo imaging |

Yuxi Ge and Gang Guo contributed equally to this work.

✉ Zhe-Wu Jin
zwjin@jiangnan.edu.cn

✉ Gen Yan
gyan@stu.edu.cn

[1] Department of Radiology, Affiliated Hospital, Jiangnan University, Wuxi 214122, Jiangsu, People's Republic of China

[2] Department of Radiology, The Second Affiliated Hospital, Xiamen Medical College, Xiamen, People's Republic of China

[3] Department of Basic Medicine, Wuxi School of Medicine, Jiangnan University, 1800 Lihu Avenue, Wuxi 214122, Jiangsu, People's Republic of China

[4] Department of Basic Medicine, Beijing University of Chinese Medicine, Beijing, People's Republic of China

## Introduction

Fibromas of the tendon sheath (FTS) are rare, benign, soft tissue tumors first described in 138 patients in 1979 [1], with few subsequent tumor and imaging studies [2]. The clinical and imaging characteristics of FTS closely resemble those of giant cell tumors of the tendon sheath (GCTTS). Both tumors are intimately associated with tendons [3] and may present as painless, slowly enlarging masses, almost exclusively in the extremities. Most FTS appear on magnetic resonance imaging (MRI) as well-defined soft tissue masses with low or variable signal intensities on T1- and T2-weighted sequences, respectively, with either no enhancement or mild to significant homogeneous enhancement on contrast-enhanced MRI [2]. Both types appear similar on MRI [4–8]. Most GCTTS appear isointense relative to the muscle on T1-weighted images, with variable intensity on T2-weighted images because of variable hemosiderin, liquid, lipid, fibrous tissue, and hemorrhagic components [9]. GCTTS show lack of or mild enhancement on contrast-enhanced MRI, similar to that of FTS [5, 6, 10, 11].

Gradient echo images are typically used to diagnose GCTTS because of susceptibility artifact, which can distinguish them from other soft tissue tumors. However, gradient echo images are easily affected by non-uniform magnetic field, so they are difficult to apply to all parts of the body. FTS consist of a dense fibrocollagenous stroma with scattered spindle-shaped fibroblasts and narrow slit-like vascular spaces [1], and GCTTS of multinucleated giant cells, foamy histiocytes, and hemosiderin-laden xanthoma cells [3, 8]. Other than gradient echo images, histopathological analysis is presently regarded as the primary method for differentiating FTS from GCTTS.

Although both FTS and GCTTS are benign, GCTTS may undergo malignant transformation or rapidly destructive progression [12, 13]. Since the first malignant giant cell tumor was described in 1979 [12], 17 patients have been reported with malignancies secondary to treatment of benign GCTTS, and 15 have been reported with primary malignant GCTTS, with four disease-related deaths. To our knowledge, malignant transformation of FTS has never been described. Therefore, MRI before surgical excision may distinguish between these two types of lesions, potentially affecting treatment decisions.

Most reports on FTS have been single case studies, and the paucity of cases has made it difficult to establish a consensus. To determine whether MRI can provide information useful for distinguishing between FTS and GCTTS, we retrospectively compared MRI data from 18 patients with histologically confirmed FTS and 24 patients with localized GCTTS. To our knowledge, this is the largest analysis of MRI features of FTS and GCTTS in the English language literature.

## Materials and methods

### Case selection

We retrospectively searched the pathology and radiology databases in our institutions to identify consecutive patients with (1) newly diagnosed histologically confirmed FTS or GCTTS and (2) clear MR images from May 2011 to May 2016. The exclusion criteria were (1) previous biopsy or surgery for FTS or GCTTS and (2) pigmented villonodular synovitis (a diffuse form of GCTTS), which was excluded through MRI because differential diagnosis between this form of GCTTS and FTS is easy.

### MRI examination

All patients underwent MRI using a 1.5-T ($n = 19$) or 3.0-T ($n = 23$) MRI scanner (Signa, GE Healthcare, USA) with either a TOSOPA phased-array coil, an EXTREM surface coil, or a GPFLEX surface coil, depending on the body part. Field of view ranged from 8 to 30 cm, slice thickness from 2 to 6 mm, and slice gap from 0 to 2.7 cm. Matrices of 256 × 128–256 were used. Axial plus sagittal and/or coronal images were obtained for all lesions. All 42 lesions underwent T1-weighted spin-echo imaging (T1WI; pulse sequences, 360–560/9–18 (TR/TE)), whereas eight underwent T2-weighted spin-echo or fast spin-echo imaging (T2WI; pulse sequences, 2200–3600/108–127 (TR/TE)). In addition, all 42 lesions underwent sagittal dual-echo proton density-weighted imaging (PDWI; pulse sequences, 2200–3600/11–29 (TR/TE)) to obtain fast spin-echo sequences. Fat-suppressed short-time inversion recovery sequences (pulse sequences, 4500–5400/48–53 (TR/TE)) were obtained for 36 lesions, and fat-suppressed T1WI images with gadolinium enhancement (0.2 mmol/kg) were obtained for 18 lesions.

### MRI and statistical analysis

All images were independently analyzed by two senior radiological diagnosticians (Yuxi Ge and Gen Yan, with 7 and 17 years of clinical experience of MR image interpretation, respectively) who were blinded to the pathological results. The demographic and clinical features assessed in the FTS and GCTTS groups included age, sex, and lesion location and diameter. The MRI features evaluated included lesion morphology (e.g., round or ovoid, lobular pattern, or casting mold; Fig. 1) and the imaging features were obtained on PDWI. The latter included the homogeneity/non-homogeneity of the signal, the presence/absence of a hypointense ring, and the location and morphology of hypointensity. Enhancing patterns on T1WI were also compared, including whether

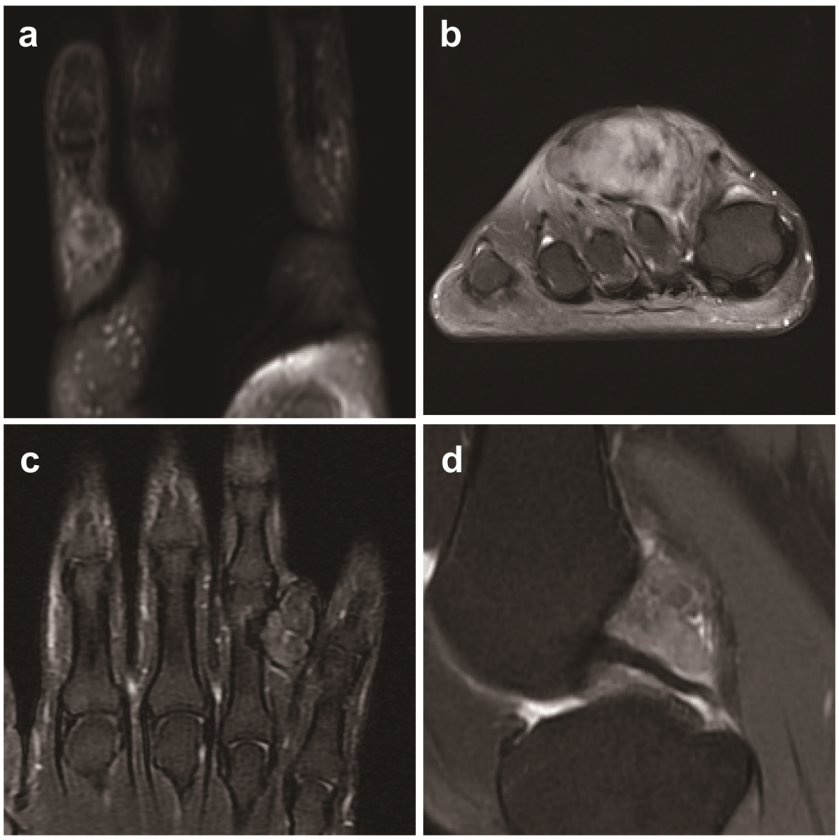


**Fig. 1** Classification and definition of the shapes of FTS and GCTTS. If the morphology of the nodule (**a**) or mass-like tumor (**b**) was oval, it was defined as an oval tumor. **c** If the morphology of the tumor was lobulated, it was classified as lobulated tumor group. **d** If the tumor was drilled into the surrounding gap, it was defined as a mold casting

enhancement was homogeneous or heterogeneous, whether the tumor crossed the joint or not, and the absorption of adjacent bone including cortical erosion or subchondral cysts. Lesions showing homogeneous signal intensity on PDWI, and homogeneous enhancement, were defined as having homogeneous signaling. The appearance of hypointense components on PDWI was defined as striped, disorderly, granular/flaky, or separated (Fig. 2). The location of hypointensity was classified as central or marginal based on the location of the low signal component; if this occurred in the periphery of the tumor, it was defined as marginal. Other locations are considered central.

All MRI findings were characterized separately by two diagnosticians who were blinded to patient outcomes, with disagreements resolved by consultation. Two weeks later, the two radiologists re-interpreted the MR features. Statistical analysis was conducted using SPSS 22.0 software (IBM Corporation). We used the chi-square tests to compare imaging findings between FTS and GCTTS, and the *t* tests to compare the age and diameter of the lesions between the two groups. A $p$ value $< 0.05$ was considered significant. Inter- and intra-observer agreements were assessed by calculating a simple kappa value for the subjective parameters. A kappa value less than 0.20 was interpreted as poor agreement, 0.21–0.40 as fair, 0.41–0.60 as moderate, 0.61–0.80 as good, and more than 0.81 as excellent agreement.

## Results

### Demographic and clinical features

We finally identified 18 patients with FTS and 24 with GCTTS. Seven cases of FTS and 12 cases of GCTTS were scanned on 1.5 T, and 11 cases of FTS and 12 cases of GCTTS on 3 T.

The 18 patients with FTS included nine men and nine women, aged 17–62 years (median 45 years). All FTS manifested clinically as painless, soft, slow-growing tissue lumps without local redness, swelling, or ulceration. One of the wrist lesions was associated with carpal tunnel syndrome symptoms, including numbness and pain in the palm and fingers. Two knee lesions were associated with recent joint soreness, and one knee and one wrist lesion were associated with mild restriction of joint activity.

The 24 patients with localized GCTTS included 13 men and 11 women, aged 15–67 years (median 43 years). All GCTTS manifested clinically as slow-growing soft tissue lumps without local redness, swelling, ulceration, or movement disorders. Three knee lesions were associated with joint soreness, and one palmar lesion was associated with local soreness and swelling. Demographic and clinical features did not differ significantly between patients with FTS and GCTTS.

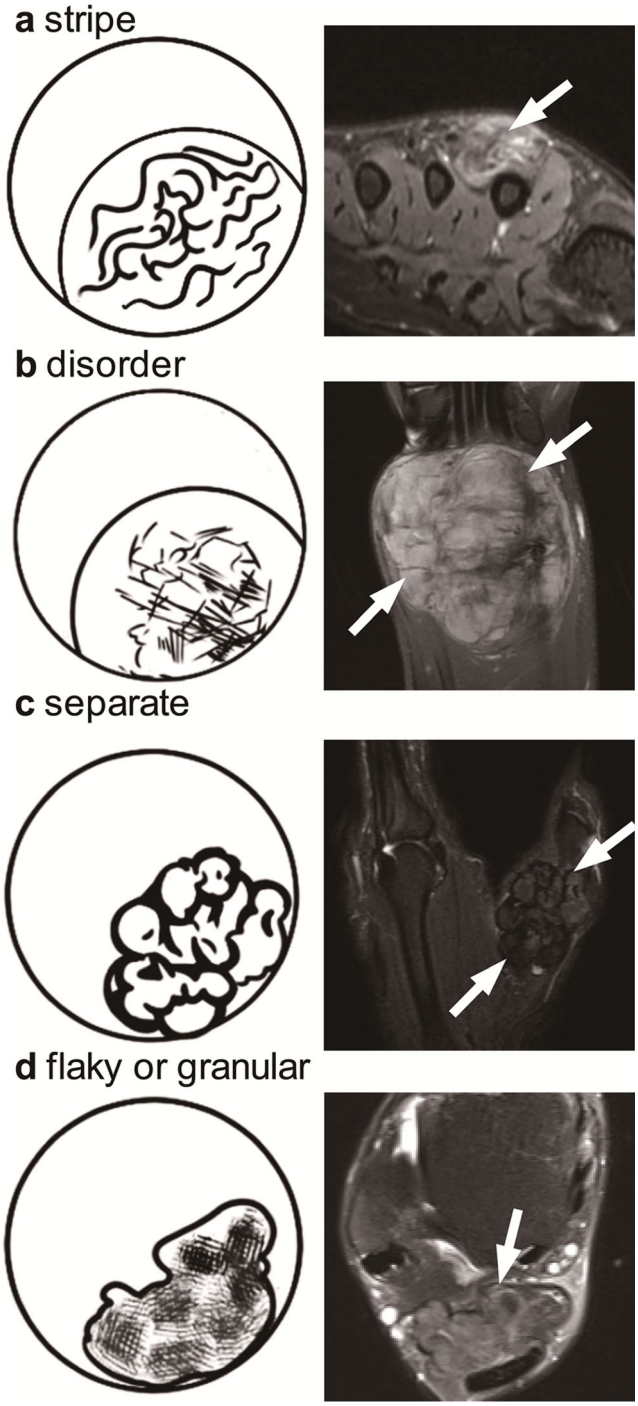


**Fig. 2** Classification and definition of the hypointensity shapes of FTS and GCTTS on PDWI. **a** The low signal components in tumors are cords and stripes. **b** The low signal components in tumors are disordered. **c** The low signal around the tumor goes inward to form a septum structure. **d** The low signal intensity in tumors is patchy or granular

## MRI features

Intra-observer and inter-observer agreements for the subjective MRI features were excellent (Table 1). The two observers agreed on the features of homogeneous signal on PDWI, bone absorption, enhancing pattern, and joint crossing in 100% of cases. The corresponding linear weighted kappa values for hypointensity ring, location of hypointensity, morphology of hypointensity on PDWI, and morphology were also high at 0.899, 0.955, 0.879, and 0.925, respectively. Intra-observer kappa values were between 0.910 and 1, showing excellent agreement.

Of the 18 FTS lesions, most were located in the palms ($n$ = 6, 33.3%), feet (4, 22.2%), and knees (4, 22.2%), followed by the wrists (2, 11.1%), shoulders (1, 5.6%), and elbows (1, 5.6%). The maximum tumor diameter ranged from 5 to 76 mm across locations, with an average of 34.7 mm. Fifteen (83.3%) lesions were round or ovoid (Fig. 3), two (11.1%) were lobular, and one (5.6%) extended into the joint or grew in casting mold, including two (11.1%) which exhibited bone erosion.

T1WI showed non-homogeneous isointensity or hypointensity relative to muscle for 16 (88.9%) lesions and homogeneous hyperintensity for two (11.1%) lesions. On PDWI, 10 (55.6%) lesions demonstrated heterogeneous hyperintensity, and eight (44.4%) exhibited heterogeneous hypointensity. Hypointense components on PDWI exhibited a striped appearance in seven (38.9%) lesions, and a disorderly appearance in 11 (61.1%) lesions (Fig. 4).

All nine lesions assessed by gadolinium-enhanced imaging showed heterogeneous enhancement (Fig. 5). Of the 24 GCTTS lesions, most were located in the palms ($n$ = 10, 41.7%) and feet (5, 20.8%), followed by the knees (4, 16.7%), wrists (2, 8.3%), ankles (2, 8.3%), and hip (1, 4.2%). The maximum tumor diameter ranged from 9 to 79 mm across locations, with an average diameter of 32.5 mm. Twelve (50%) lesions were lobular, five (20.8%) were oval-shaped, and seven (29.2%) extended into the joint or grew in casting mold (Fig. 3). More than half these lesions showed bone erosion (Fig. 3c).

PDWI showed homogeneous signaling in seven (29.2%) lesions and heterogeneous lesions in 17 (70.8%, Fig. 4c). The seven lesions with homogeneous signals exhibited isointensity or hypointensity compared with muscle on T1WI, and hyperintensity on PDWI. Hypointense signals on PDWI, which were granular/flaky or septum-like for 13 lesions (Fig. 4d, e) and were located near the periphery of the tumor in eight lesions, were apparent for the other 17 lesions that showed heterogeneous signaling. PDWI showed complete or incomplete hypointense rings found around 14 lesions.

Of the nine lesions that underwent gadolinium-enhanced imaging, six showed homogeneous enhancement (Fig. 5).

## Statistical comparisons of MR features

Imaging features differed significantly between PDWI and other MRI sequences (Table 2). FTS and GCTTS differed

**Table 1** Intra-observer and inter-observer agreements for the subjective MRI features

| MRI features | Kappa values of intra-observer (agreement number/total) | | Kappa values of inter-observer (agreement number/total) |
|---|---|---|---|
| | Observer1 | Observer2 | |
| PDWI | | | |
| Homogeneous | 1 | 1 | 1 |
| Hypointensity ring | 0.950 | 1 | 0.899 |
| Location of hypointensity | 0.955 | 1 | 0.955 |
| Morphology of hypointensity | 0.969 | 0.910 | 0.879 |
| Other sequences | | | |
| Morphology | 1 | 1 | 0.925 |
| Bone absorption | 1 | 1 | 1 |
| Enhancing pattern | 1 | 1 | 1 |
| Cross the joint | 1 | 1 | 1 |

The two observers agreed on the features of homogeneous signal on PDWI, bone absorption, enhancing pattern, and joint crossing in 100% of cases. The corresponding linear weighted kappa values for hypointensity ring, location of hypointensity, morphology of hypointensity on PDWI, and morphology were also high at 0.899, 0.955, 0.879, and 0.925, respectively. Intra-observer kappa values were between 0.910 and 1, showing excellent agreement

significantly in their degree of lesion morphology ($p < 0.001$), prevalence of bone absorption ($p = 0.008$), presence of a hypointense ring ($p = 0.006$), signal homogeneity ($p < 0.001$), and location and morphology of hypointensity ($p < 0.001$).

### Diagnostic performance for differentiating FTS from GCTTS

Using the characteristics of lesion shape, location, and signal, 38 of 42 cases (90%) were correctly classified as either FTS or GCTTS based on a combination of the two features of homogenous signal and hypointensity shape on PDWI (Fig. 6). The remaining four cases were all GCTTS, with more complex low signal patterns that were difficult to differentiate from FTS. Additional features may have utility for differential diagnosis: central location of hypointensity, and striped or disordered shape of hypointensity on PDWI revealed 100% sensitivity for FTS. For other characteristics, the sensitivities, specificities, and diagnostic accuracies ranged from 83 to 100%, 29 to 79%, and 60 to 89%, respectively (Table 3).

## Discussion

Although the MRI features of FTS and GCTTS are similar, our results highlight differences. First, FTS give a non-uniform signal on the PDWI sequence; tumors with uniform signal are more likely to be GCTTS. Second, the low signal patterns of the two tumor types in PDWI differ: FTS are strip-like or irregular, while GCTTS are predominantly flaky/granular or separated. Combining these

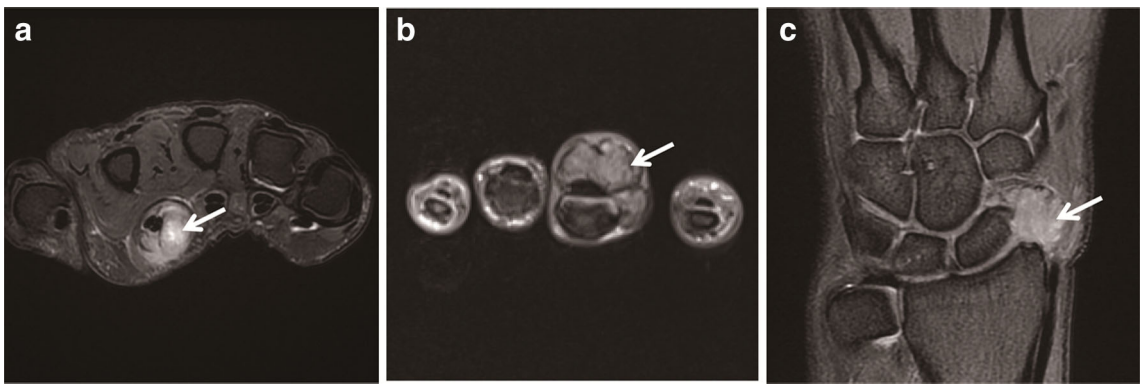


**Fig. 3** Morphological comparison of FTS and GCTTS. **a** Representative images of oval-shaped of FTS. MRI in a 55-year-old woman shows an oval nodule with a high signal around the flexor tendon (arrow). **b** Images of separated shape of GCTTS. Axial PDWI of a 22-year-old woman, a lobulated high-signal tumor is revealed around the extensor tendon (**c**) images of casting mold of GCTTS. Coronal PDWI of a 61-year-old man, a cast-shaped high-signal tumor, accompanied by bone absorption of the scaphoid, is shown around the wrist

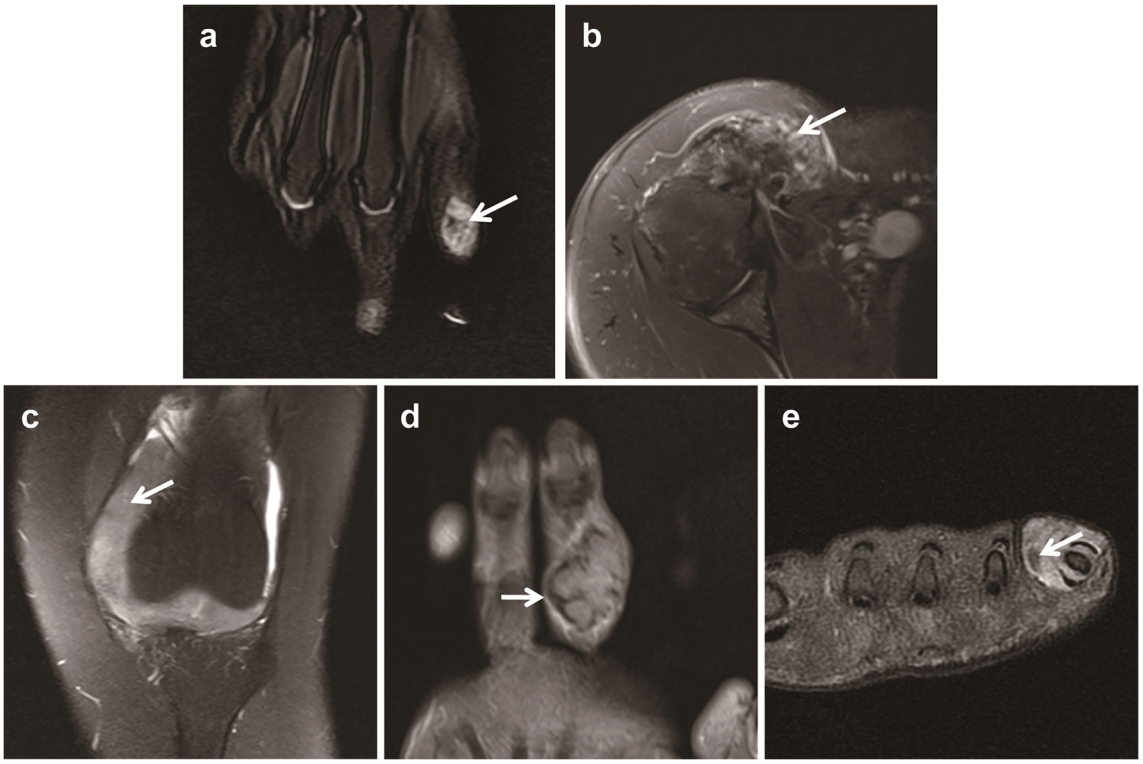


**Fig. 4** Low signal morphology comparison between FTS and GCTTS on PDWI. **a** Representative images of stripe hypointensity of FTS. MRI in a 25-year-old woman shows strip-like low signal in the nodule on the index finger (arrow). **b** Images of disordered hypointensity of FTS. A 44-year-old woman demonstrates irregularly arranged low signal in the lesion of the shoulder (arrow). **c** The image of homogenous signal of GCTTS. A 26-year-old male with an even hyperintensity on the knee (arrow). **d** Image of separated hypointensity of GCTTS. A visible separately low signal on the edge of the lesion at the finger was shown in a 31-year-old female (arrow). **e** Image of granular low signal of GCTTS. A 62-year-old female patient showed a granular low signal in a lesion on the small toe (arrow)

two characteristics enabled us to classify 90% of tumors correctly as FTS or GCTTS. Third, FTS are predominantly round or ovoid, and GCTTS are cast and lobulated. Finally, other signs that suggest GCTTS include low signal on the PDWI located near the periphery of the tumor, and a low signal ring were found, bone resorption, uniform enhancement, and cross-articular.

Morphologically, most FTS in our study were round or ovoid [14], whereas most GCTTS were lobulated or exhibited a casting mold pattern, consistent with the literature [15]. FTS are histologically characterized by a dense fibrocollagenous stroma with scattered spindle-shaped fibroblasts and narrow, slit-like vascular spaces [1] with a hard texture. Consequently, these lesions appear nodular and mass-like. In contrast, most GCTTS are characterized by the presence of histiocytes, monocytes, multinucleated giant cells, foam cells, hemosiderin-laden macrophages, and siderophages, with fissures of different shapes, false glandular spaces, and pseudoacinar structures. Because their cellular morphology is diverse and loosely arranged, GCTTS that grow in a joint cavity or between bones may exhibit a casting mold pattern. Some GCTTS wrap around the fibrous capsule, which can extend deeper into the tumor and result in a lobulated appearance.

Although both FTS and GCTTS have been reported to cause absorption of adjacent bone, only a few cases of FTS with bone erosion have been described [5]. In contrast, the incidence of bone erosion is higher with GCTTS [16]. One case series reported bone erosion associated with only 14% of GCTTS [17], in contrast to our findings of cortical erosion or subchondral cysts in 12 of 24 GCTTS lesions, and bone erosion or cysts in 2 of 18 FTS lesions. The relatively high proportion of GCTTS with bone erosion (50%) that we report may be due to both our small sample size and different imaging methods. Bone erosion may be caused by tumor compression in patients with FTS whereas GCTTS lesions contain macrophages, which function as osteoclasts that dissolve cortical bone and form a cavity on the bone surface [18]. GCTTS were thus more likely to cause bone erosion and surrounding destruction, more extensively so when malignant [19].

PDWI showed a complete or incomplete hypointense ring around the lesion in three (16.7%) of our 18 patients with FTS, a finding that may be related to the thin or absent envelope on FTS. In contrast, for 14 (58.3%) of the 24 GCTTS lesions, PDWI showed a hypointense ring that extended into the tumor and formed a separate, cauliflower-like structure. The morphological features of GCTTS may be attributed to a fibrous envelope on the surface of the lesion.

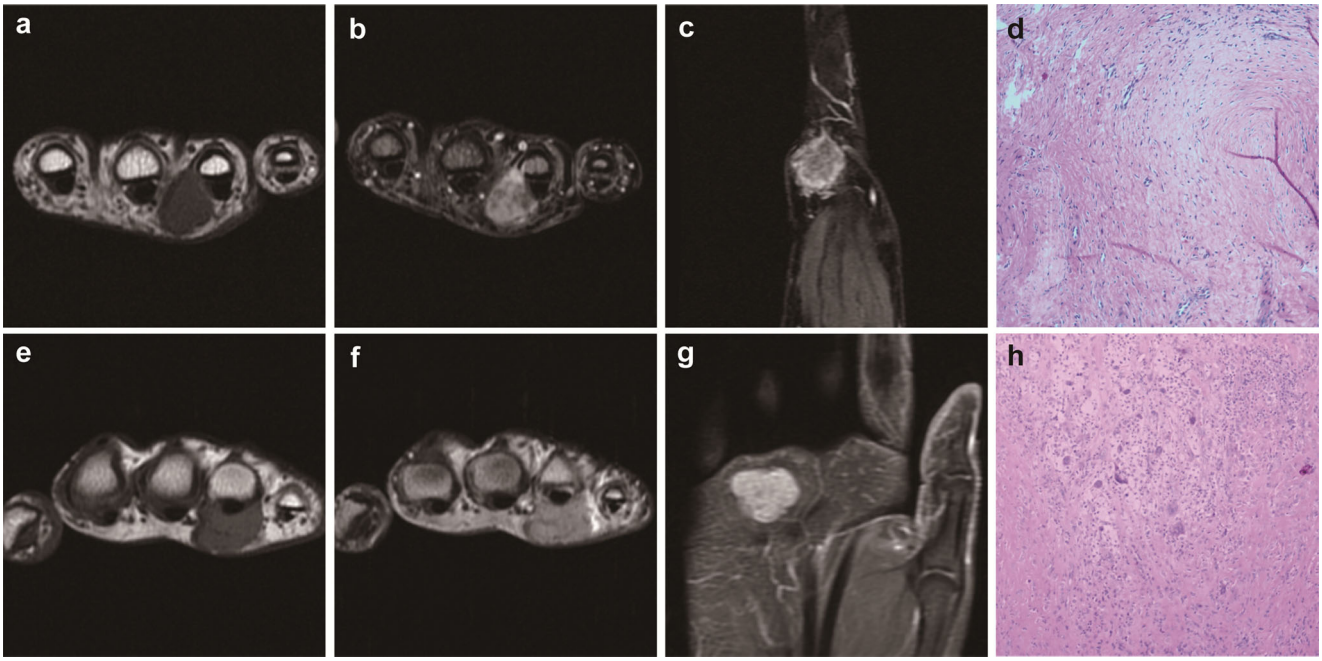


**Fig. 5** Comparison of MRI enhancement between FTS and GCTTS. a–d Representative images of FTS enhancement. MRI in a 61-year-old female demonstrates a low signal nodule on the dorsal side of the 4th finger on axial T1-weighted image (**a**). Contrast-enhanced MR image of axial (**b**) and sagittal (**c**) T1-weighted image shows an uneven enhancement lesion. Staining of the lesion with hematoxylin and eosin (original magnification, × 100) (**d**), showing spindle-shaped tumor cells surrounded by a dense fibrocollagenous stroma with narrow, slit-like vascular spaces. **e**–**h** Representative images of GCTTS enhancement. MRI in a 47-year-old male demonstrates a low signal nodule on the dorsal side of the 4th finger on axial T1-weighted image (**e**). Contrast-enhanced T1-weighted MR axial (**f**) and coronal (**g**) images show a homogeneously enhanced lesion. Staining of the lesion with hematoxylin and eosin (original magnification, × 100) (**h**), showing histiocyte-like mononuclear cells, foamy cells, a small number of multinuclear giant cells, and collagen fibers infiltrating the interstitial space

Although both FTS and GCTTS demonstrate hypointensity on PDWI, the morphology and distribution of the hypointense components distinguish the two lesion types. FTS showed striped or disordered hypointensity on T2WI, probably due to the presence of dense collagen fiber bundles with a low $H^+$ content. In some patients, T2WI/PDWI results were characterized by hypointensity, mainly because these tumors contain multiple collagen bundles. In our study, hypointensity on PDWI appeared striped in seven (38.9%) and disorderly in 11 (61.1%) FTS, with all hypointense areas at the center of the lesion, probably because most spindle cells were present at the center [1]. In contrast, GCTTS demonstrated granular and separated hypointensity on PDWI, which may have been due to the deposition of the paramagnetic compound caused by repeated bleeding [20]. We found that 76.4% (13/17) of non-homogeneous GCTTS lesions demonstrated granular/flaky or separated hypointensity on PDWI. This hypointensity was scattered or located at the periphery of the lesion, perhaps because foam cells can engulf hemosiderin, which is patchy or nested, and is located around the lesion [1].

Although both FTS and GCTTS may demonstrate mild to significant enhancement on gadolinium-enhanced MRI [2, 14], their enhancement patterns differ completely. We found that FTS lesions exhibited heterogeneous enhancement of mild to high intensity and primarily dependent on their proportions of collagen fibers, which are not enhanced on enhanced MRI sequences. In contrast, nine GCTTS lesions that underwent contrast-enhanced imaging demonstrated mild to high intensity, with six lesions showing homogeneous enhancement despite the presence of hypointensity at the periphery. Similarly, Beuckeleer et al [15] described strong homogeneous enhancement in ten of 13 GCTTS, possibly due to blood vessel proliferation in the GCTTS lesions.

We found that patient age and sex, as well as lesion size and location, did not differ significantly in the FTS and GCTTS groups. However, FTS occur more frequently in male adults (peak age, 30–50 years), predominantly in the upper limbs [1]. They reported that 82% of fibromas of the tendon sheaths occurred in the fingers, hands, and wrists, and seven cases were found extra-articularly around the knee joint. FTS occurring around large joints such as the elbows, shoulders, hips, knees, and ankles are rarely reported [21]. However, in our study, 8/18 cases of FTS occurred in large joints. Of these lesions, two were intra-articular FTS in the knee joint. A further 44% were located in the fingers, hands, and wrists. This may be due to small sample size and referral bias to our institution, and if the lesion is too small, magnetic resonance examination may not be performed in our unit. Therefore, some hand lesions may have been excluded from our study. Our

**Table 2** MRI features of patients diagnosed with FTS and GCTTS

| MRI feature | FTS ($n = 18$) | GCTTS ($n = 24$) | Chi-square test ($p$ value) |
|---|---|---|---|
| Morphology | | | |
| Oval like | 15 | 5 | < 0.001* |
| Lobulated | 2 | 12 | |
| Casting mold | 1 | 7 | |
| Bone absorption | | | |
| Yes | 2 | 12 | 0.008* |
| No | 16 | 12 | |
| Hypointensity ring on PDWI | | | |
| Yes | 3 | 14 | 0.006* |
| No | 15 | 10 | |
| Homogeneous on PDWI | | | |
| Yes | 0 | 7 | < 0.001* |
| No | 18 | 17 | |
| Morphology of hypointense on PDWI | | | |
| Striped | 7 | 2 | < 0.001* |
| Disorderly | 11 | 2 | |
| Granular/flaky or septated | 0 | 13 | |
| Location of hypointensity on PDWI | | | |
| Margin | 0 | 8 | < 0.001* |
| Central | 18 | 9 | |

*Statistically significant

data show an average age of patients with FTS of 42.8 ± 4.37, consistent with the literature. In contrast, GCTTS occur more frequently in the hands and feet of women aged 31–40 years [8], also in accordance with our findings.

Involvement of the tenosynovial space was detected in nine of 10 localized GCTTS [22], leading to a conclusion that MR imaging is useful in assessing tumor extent and involvement of the joint and tenosynovial space. Similarly, our data show that nine of the 24 patients with GCTTS had lesions that crossed the joint longitudinally. Lesion range and size should therefore be evaluated in patients diagnosed with GCTTS, with resection extended during surgery as required. Preoperative MRI examination is important for differential diagnosis of FTS and GCTTS, and MRI is an important tool for postoperative follow-up assessments.

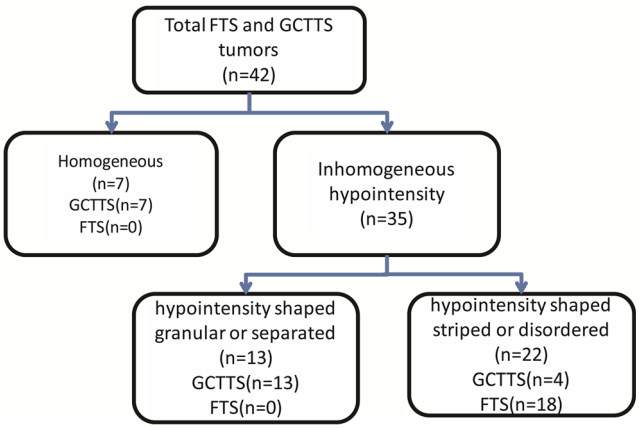


**Fig. 6** Classification of FTS and GCTTS based on the major imaging findings (homogeneity of signal and shape of hypointensity on PDWI). Among all patients, 18/18 FTS and 20/24 GCTTS were correctly differentiated in our analyses, and four cases of GCTTS remained unclassifiable. Accuracy was thus 90%

Among all 18 cases of FTS and 24 cases of GCTTS, across small and large joints, many MRI characteristics were shared by tumors of various sizes and locations. For FTS, the imaging features of even small finger lesions shared the characteristic features, with heterogeneous oval masses with low signal in a striped or disordered shape in the center of the lesion on PDWI sequence. GCTTS involving small joints such as the hand or foot often appeared as lobulated lesions surrounded by a low signal ring, with the low signal components separated or granular/flaky. However, GCTTS in large joints such as the knee and wrist tended towards mold shape and homogeneous signals.

Kappa values for the intra- and inter-observer agreements were lowest for PDWI sequences with low signal patterns, but were nonetheless 0.879. Four disagreements between the two observers resulted from confusion between flaky and irregular shape. This suggests that the clinical experience of observers is important for differential diagnosis of these two tumor types.

Limitations of our study include first its retrospective nature and use of images obtained from different scanners with inconsistent imaging protocols. For example, T2 fat-saturated images, STIR images, and gradient echo images, all of which may be helpful in differential diagnosis of these two tumor types, are not available at our institution. It is uncertain whether our results are applicable to fluid-sensitive MRI sequences other than PDWI, which is not always available for imaging of soft tissue masses. Second, the rarity of FTS restricted our

**Table 3** Diagnostic performance of FTS MRI features

| MRI features of FTS | Sensitivity (%) | Specificity (%) | PPV (%) | NPV (%) | Accuracy (%) |
|---|---|---|---|---|---|
| PDWI | 100 | 29 | 51 | 100 | 60 |
| Inhomogeneous | | | | | |
| Central location of hypointensity | 100 | 47 | 67 | 100 | 74 |
| Striped or disordered shape of hypointensity | 100 | 76 | 82 | 100 | 89 |
| Other sequences | 83 | 79 | 75 | 86 | 81 |
| Nodule/mass-like morphology | | | | | |
| Inhomogeneous enhancing pattern | 100 | 67 | 75 | 100 | 83 |

sample size, particularly for the enhanced MR cases. This may have introduced bias in our summaries of the MR features of FTS. Third, the blinded observers had participated in patient diagnosis in daily practice; hence, recall bias might have occurred.

In conclusion, MR imaging depicts the characteristics of FTS and GCTTS. Characteristics useful for discriminating between FTS and GCTTS appear to be a non-homogeneous, low-intensity signal with a stripe or irregular shape on PDWI, round or oval shape, and uneven enhancement. Although MRI differences between FTS and GCTTS are sensitive and specific enough to differentiate between the two lesions, confirmatory histological diagnosis is still recommended.

**Funding** This study has received funding by the Natural Science Foundation of Jiangsu Province (No. BK20151106), Wuxi Key Medical Talents (ZDRC032), and Public Health Research Center at Jiangnan University (No. JUPH201501).

## Compliance with ethical standards

**Guarantor** The scientific guarantor of this publication is Gen Yan, M.D., Ph.D.

**Conflict of interest** The authors of this manuscript declare no relationships with any companies, whose products or services may be related to the subject matter of the article.

**Statistics and biometry** Yinghua Xuan kindly provided statistical advice for this manuscript.

**Informed consent** Written informed consent was waived by the Institutional Review Board.

**Ethical approval** Institutional Review Board approval was obtained.

**Methodology**
- Retrospective
- Case-control study
- Performed at one institution

## References

1. Chung EB, Enzinger FM (1979) Fibroma of tendon sheath. Cancer 44:1945–1954
2. Moretti VM, de la Cruz M, Lackman RD, Fox EJ (2010) Fibroma of tendon sheath in the knee: a report of three cases and literature review. Knee 17:306–309
3. Weiss SW, Goldblum JR (2005) Soft tissue tumors, 5th edn. Elsevier Mosby, Philadelphia
4. Glover MK, Chebib I, Simeone FJ (2014) Intra-articular fibroma of tendon sheath arising in the acromioclavicular joint. Skeletal Radiol 43:681–686
5. Hitora T, Yamamoto T, Akisue T et al (2002) Fibroma of tendon sheath originating from the knee joint capsule. Clin Imaging 26: 280–283
6. Kundangar R, Pandey V, Acharya KK, Rao PS, Rao L (2011) An intraarticular fibroma of the tendon sheath in the knee joint. Knee Surg Sports Traumatol Arthrosc 19:1830–1833
7. Solomou A, Kraniotis P (2017) Giant cell tumor of the tendon sheath of the tendinous insertion in pes anserinus. Radiol Case Rep 12:353–356
8. Gouin F, Noailles T (2017) Localized and diffuse forms of tenosynovial giant cell tumor (formerly giant cell tumor of the tendon sheath and pigmented villonodular synovitis). Orthop Traumatol Surg Res 103(S 1):91–97
9. Parmar HA, Sitoh YY, Tan KK, Teo J, Ibet SM, Hui F (2004) MR imaging features of pigmented villonodular synovitis of the cervical spine. AJNR Am J Neuroradiol 25:146–149
10. Sookur PA, Saifuddin A (2011) Indeterminate soft-tissue tumors of the hand and wrist: a review based on a clinical series of 39 cases. Skeletal Radiol 40:977–989
11. Fox MG, Kransdorf MJ, Bancroft LW, Peterson JJ, Flemming DJ (2003) MR imaging of fibroma of the tendon sheath. AJR Am J Roentgenol 180:1449–1453
12. Bertoni F, Unni KK, Krishnan MBBS, Beabout JW, Sim FH (1997) Malignant giant cell tumor of the tendon sheaths and joints (malignant pigmented villonodular synovitis). Am J Surg Pathol 21:153–163
13. Righi A, Gambarotti M, Sbaraglia M et al (2015) Metastasizing tenosynovial giant cell tumour, diffuse-type/pigmented villonodular synovitis. Clin Sarcoma Res 5:15. https://doi.org/10.1186/s13569-015-0030-2 eCollection 2015
14. Sayit AT (2014) Localized giant cell tumors of the flexor tendon sheath of the finger: an analysis of twenty five patients. J Clin Anal Med 7:188–192
15. De Beuckeleer L, De Schepper A, De Belder F, Van Goethem J, Marques MCB, Broeckx J, Vermaut F (1997) Magnetic resonance imaging of localized giant cell tumour of the tendon sheath (MRI of localized GCTTS). Eur Radiol 7:198–201
16. Palmerini E, Staals EL, Maki RG et al (2015) Tenosynovial giant cell tumour/pigmented villonodular synovitis: outcome of 294 patients before the era of kinase inhibitors. Eur J Cancer 51:210–217
17. Karasick D, Karasick P (1992) Giant cell tumor of the tendon sheath: spectrum of radiological findings. Skeletal Radiol 21:219–224
18. Neale SD, Kristelly R, Gundle R, Quinn JM, Athanasou NA (1997) Giant cells in pigmented villo nodular synovitis express an osteoclast phenotype. J Clin Pathol 50:605–608
19. Li CF, Wang JW, Huang WW et al (2008) Malignant diffuse-type tenosynovial giant cell tumors: a series of 7 case comparing with 24 benign lesions with review of the literature. Am J Surg Pathol 32:587–599
20. Ho CY, Maleki Z (2012) Giant cell tumor of tendon sheath: cytomorphologic and radiologic findings in 41 patients. Diagn Cytopathol 40(S2):E94–E98
21. Suzuki K, Yasuda T, Suzawa S, Watanabe K, Kanamori M, Kimura T (2017) Fibroma of tendon sheath around large joints: clinical characteristics and literature review. BMC Musculoskelet Disord 18:376
22. Kitagawa Y, Ito H, Amano Y, Sawaizumi T, Takeuchi T (2003) MR imaging for preoperative diagnosis and assessment of local tumor extent on localized giant cell tumor of tendon sheath. Skeletal Radiol 32:633–638